A Clinically Practical Method to Acquire Parametric Images of Unidirectional Metabolic Rates and Blood Spaces

Wai-Hoi Wong and Keri Hicks

Department of Nuclear Medicine, University of Texas M. D. Anderson Cancer Center, Houston, Texas

As SPECT imaging has become more quantitative with the advent of the attenuation correction, SPECT parametric imaging can become a reality if the data acquisition and the numeric reduction procedures can be simplified. **Methods:** A method that is clinically practical for acquiring quantitative parametric images of unidirectional metabolic rate constants and apparent blood space is proposed. Its application to PET imaging with FDG was investigated. This procedure requires a short postinjection waiting period, three sequential imaging scans and one blood sample (1 ml) during each scan, obviating the requirements of continuous blood sampling, "assumed" rate constants (autoradiographic method) and difficult nonlinear regression computations. The effect of the early-phase blood input function is computed directly from the image. The clinical procedure is completed 1 hr after FDG injection. The computation time for generating 21 metabolic rate image slices and blood space slices is negligible (30 sec after image reconstruction). Preliminary human studies on brain, heart, liver and tumor were performed. **Results:** The method was tested on seven normal subjects. The results showed that the rapidly changing early-phase blood input can be derived from the raw image and that the metabolic rate images of this method agreed with the results from the graphical analysis method, using continuous sampling, and with published data from three-compartment models. **Conclusion:** This study is clinically more practical and computationally simpler as a method to acquire parametric images of the metabolic rate constant, K_i, and the apparent blood space V_d for unidirectional tracers. Applying this simple quantitative parametric imaging method to routine clinical studies may improve the accuracy of routine clinical evaluations.

Key Words: PET; SPECT; modeling; metabolism

J Nucl Med 1994; 35:1206–1212

The ability to generate quantitative parametric images with SPECT and PET using physiologic modeling techniques is desirable but not always clinically practical. A simple technique is proposed that generates images of the macrometabolic rate constant K_i into the tissue-bound compartment ($K_i = K_1k_3/[k_2 + k_3]$ in the three-compartment transport model) and apparent blood space activity. The application of this method with the ^{18}F-fluorodeoxyglucose (FDG) tracer was studied in this investigation.

Currently, there are three methods that generate parametric images of K_i for FDG: (1) the three-compartment model technique (*1–3*); (2) the autoradiographic technique (*1–5*); and (3) the graphical analysis technique (*6,7*). The three-compartment model and the graphical analysis technique can generate images of K_i and the apparent blood space; the autoradiographic technique can generate K_i. The autoradiographic technique is the easiest to implement because of its mathematic simplicity, but "normal tissue" rate constants, K_1, k_2 and k_3, which have to be assumed for all tissue, may not be valid, e.g., for tumors whose rate constants may be substantially different from those of normal tissue. The three-compartment model requires many time-serial images and is demanding computationally, with hours of nonlinear-regression curve fitting to derive a set of parametric images.

The graphical analysis method uses a much less demanding linear-regression curve-fitting procedure for each pixel (computation time on the authors' work station is about 3 min for 21 128 × 128 image slices). All three methods require continuous sampling of blood, beginning immediately postinjection, until the end of the imaging period. In a typical FDG study, there may be 25 or more blood samples to collect, spin, weigh, count and input into a computer, tasks that require trained staff. Automatic blood sampling systems can alleviate some of the chores, but these systems are generally custom built (*8,9*), waste blood and have difficulty performing plasma separations. Hence, parametric images are not routinely generated in busy clinical environments.

The purpose of this study was to develop a clinically practical modeling technique to acquire parametric images of the tracer macrometabolic rate constant K_i and blood space activity. The goal was to simplify the blood sampling and computational requirements so that, without requiring additional staff, the images of K_i and blood pool could be generated immediately after the completion of raw image reconstruction.

Received July 21, 1993; revision accepted Mar. 3, 1994.

For correspondence or reprints contact: Wai-Hoi Wong, PhD, Department of Nuclear Medicine, Box 59, University of Texas M. D. Anderson Cancer Center, 1515 Holcombe Blvd., Houston, TX 77030.

MATERIALS AND METHODS

The proposed method was based on the concept of mass balance of unidirectional (trapped) tracers, which is also the basis for the graphical analysis technique (*6,7*). In graphical analysis, the tissue activity (normalized for a constant blood-tracer input) is plotted against the integrated blood-tracer input function (also normalized for a constant input). The slope of the normalized uptake is the tracer macrometabolic rate constant K_i of the tissue-bound space, and the intercept, V_d, is related to the blood distribution space and vascular volume. Because there are only two unknowns (K_i and V_d), the minimal number of time-activity image sets required to solve for K_i and V_d in the graphic method is two.

In this proposed method, three time-series images are acquired (instead of two) because the initial blood input function A(t) is going to be solved from the raw images directly. Solving for A(t) directly from the raw images eliminates frequent blood sampling in the initial period, which is essential if a procedure is to be clinically practical.

After a short waiting period during which the total blood space equilibrates with blood and with a knowledge of the raw image pixel data at times t_2, t_3 and t_4, Equations 1, 2 and 3 for computing K_i and V_d can be derived from the mass balance of unidirectional tracers (the variables are depicted in Fig. 1) as

$$T_2 - K_i\left[\int_0^{t_2} A(u)\,du\right] - A_2V_d = 0, \quad \text{Eq. 1}$$

$$T_3 - K_i\left[\int_0^{t_2} A(u)\,du + \int_{t_2}^{t_3} A(u)\,du\right] - A_3V_d = 0, \quad \text{Eq. 2}$$

$$T_4 - K_i\left[\int_0^{t_2} A(u)\,du + \int_{t_2}^{t_3} A(u)\,du + \int_{t_3}^{t_4} A(u)\,du\right] - A_4V_d = 0, \quad \text{Eq. 3}$$

where T_2, T_3 and T_4 are the tissue activities during scans A, B and C and A_2, A_3 and A_4 are the blood activities at times t_2, t_3 and t_4. The blood integrals can be written in terms of the variables, dc_1, dc_2 and dc_3, where

$$dc_1 = \int_0^{t_2} A(u)\,du, \quad \text{Eq. 4}$$

$$dc_2 = \int_{t_2}^{t_3} A(u)\,du, \quad \text{Eq. 5}$$

$$dc_3 = \int_{t_3}^{t_4} A(u)\,du. \quad \text{Eq. 6}$$

By substitution, Equations 1 to 3 can be expressed as

$$T_2 - K_i[dc_1] - A_2V_d = 0, \quad \text{Eq. 7}$$

$$T_3 - K_i[dc_1 + dc_2] - A_3V_d = 0, \quad \text{Eq. 8}$$

$$T_4 - K_i[dc_1 + dc_2 + dc_3] - A_4V_d = 0. \quad \text{Eq. 9}$$

In this three time-scan strategy, the three time integrals (dc_1, dc_2 and dc_3), not the detailed time dependence of the blood input function, are important. Because blood is sampled at a late phase at which the blood activity varies slowly, dc_2 and dc_3 can be easily calculated by either linear or second-order polynomial interpolation of the three blood samples, A_2, A_3 and A_4. A linear interpolation is used in this study. The initial rapidly changing blood input function that normally needs to be sampled most frequently is not measured in this method because only its integral (dc_1) is manifested in the model and the integral dc_1 is treated as an unknown to be solved in this method. The three unknowns (dc_1, K_i and V_d) in Equations 7, 8 and 9 can be expressed for each pixel as

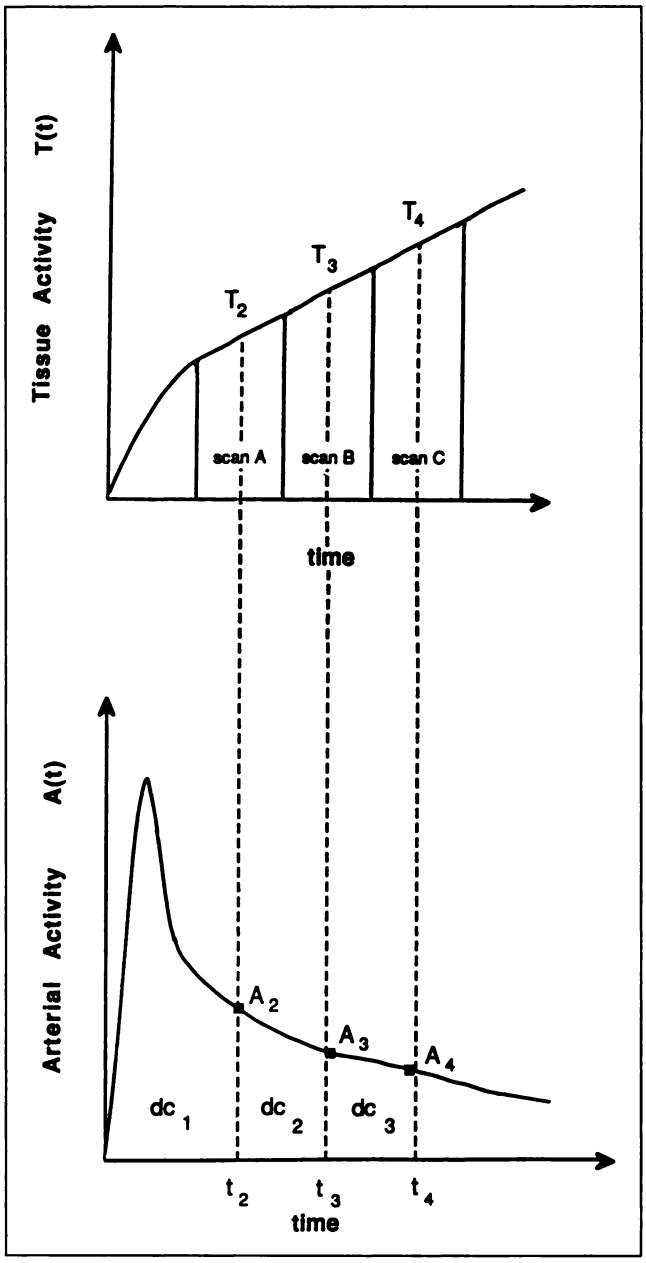

FIGURE 1. Illustration of the mathematic symbols used: T_2, T_3 and T_4 are average tissue activities in scan A, B and C, respectively. A_2, A_3 and A_4 are the arterialized venous blood activities at the midpoint of scan A, B and C, respectively. The integral of the blood curve from injection time to time t_2, (midtime of scan A) is represented by dc_1. The blood integrals from t_2 to t_3 (midtime of scan B) and from t_3 to t_4 (midtime of scan C) are represented by dc_2 and dc_3, respectively.

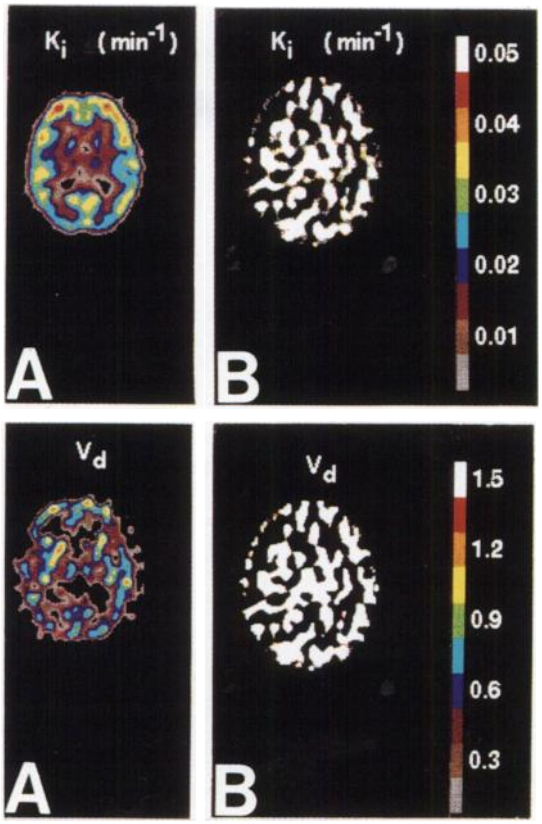

FIGURE 2. (A) K_i and V_d images using the derived grand mean of the initial blood input, dc_1. (B) K_i and V_d images using the individual pixel dc_1.

$$dc_1 = \frac{(T_4A_2dc_2 - T_3A_2dc_2 - T_3A_2dc_3 + A_3T_2dc_2 + A_3T_2dc_3 - A_4T_2dc_2)}{(T_4A_3 - T_4A_2 + T_3A_2 - A_3T_2 - A_4T_3 + A_4T_2)}, \quad \text{Eq. 10}$$

$$K_i = \frac{(T_4A_3 - T_4A_2 + T_3A_2 - A_3T_2 - A_4T_3 + A_4T_2)}{(-A_2dc_3 + A_3dc_2 + A_3dc_3 - A_4dc_2)}, \quad \text{Eq. 11}$$

$$V_d = \frac{(T_3dc_2 + T_3dc_3 - T_4dc_2 - T_2dc_3)}{(-A_2dc_3 + A_3dc_2 + A_3dc_3 - A_4dc_2)}. \quad \text{Eq. 12}$$

Ideally, if all the known values T_2, T_3, T_4, A_2, A_3 and A_4 have no measurement or statistical errors, Equations 10 to 12 can be evaluated exactly for each pixel to determine dc_1, K_i and V_d. However, because these measured values can have large uncertainties, in particular the tissue uptakes (T_2, T_3 and T_4) measured by PET, the following strategy with appropriate constraints is used.

The first parameter to be determined is dc_1, the initial blood activity integral, which is then used for the determination of K_i and V_d. Assuming all the pixels in the imaged organs have the same arterial activity over time, all the pixels will have the same blood activity integral dc_1. Every pixel within the imaged object, therefore, provides an independent estimation of dc_1, which can be determined accurately by taking a mean value of dc_1 over thousands of pixels. The procedure for finding dc_1 is as follows. First, the preliminary K_i and V_d are computed without any knowledge of dc_1 from Equations 11 and 12 for each pixel within the imaged object over the entire set of transverse images. Second, for each pixel, the blood input dc_1 can be computed, using the preliminary pixel K_i and V_d values from the first step, by the following equations (from Equations 7, 8 and 9)

$$dc_1(i, j, t_2) = [(T_2 - A_2V_d)/K_i], \quad \text{Eq. 13}$$

$$dc_1(i, j, t_3) = [(T_3 - A_3V_d)/K_i] - dc_2, \quad \text{Eq. 14}$$

$$dc_1(i, j, t_4) = [(T_4 - A_4V_d)/K_i] - dc_2 - dc_3, \quad \text{Eq. 15}$$

where i and j are the x and y location indices of the chosen pixel. From Equations 13 to 15, it is obvious that, first, if there are measurement errors in the tissue and blood, the errors in computing the blood input $dc_1(i, j, t)$ will be high if K_i is near zero (i.e., division by zero). The imposition of a lower threshold, K_i(chest) more than 0.002 and K_i(brain) more than 0.008/min, allows the computation to avoid this numerically sensitive region. These thresholds are empirically determined from normal subjects with continuous blood sampling such that the derived dc_1 matched the dc_1 measured from continuous blood sampling data. Second, the condition, V_d greater than 0, is used because negative blood space values are physically incorrect, which may indicate bad data points. Hence, only pixels that satisfy these two constraints of V_d and K_i are used to calculate the mean dc_1. Solving Equation 13, for each chosen pixel (i, j), the local pixel $\langle dc_1(i, j)\rangle$ is obtained.

The grand estimate for dc_1 from all the chosen pixels in the image set is

$$\langle\langle dc_1\rangle\rangle = \sum \langle (dc_1(i, j))\rangle / [\text{number of chosen pixels}]. \quad \text{Eq. 16}$$

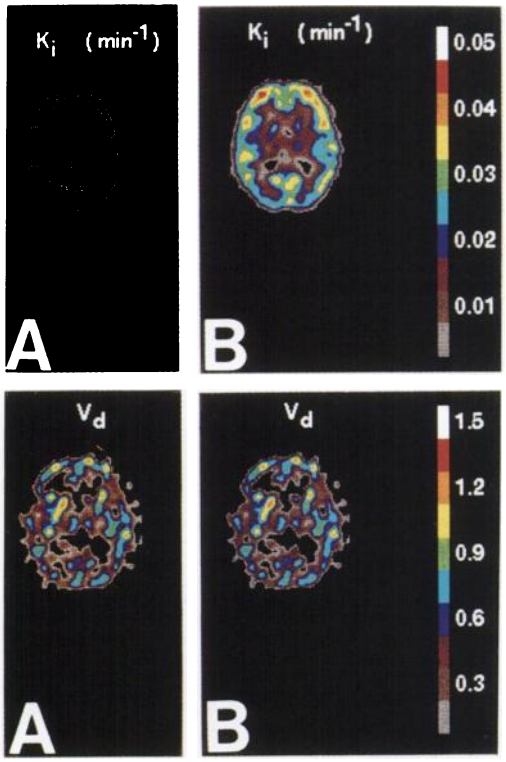

FIGURE 3. (A) K_i and V_d images derived from regular graphical analysis with continuous venous blood sampling (35 samples). (B) K_i and V_d images with this proposed method using three late-phase venous blood samples.

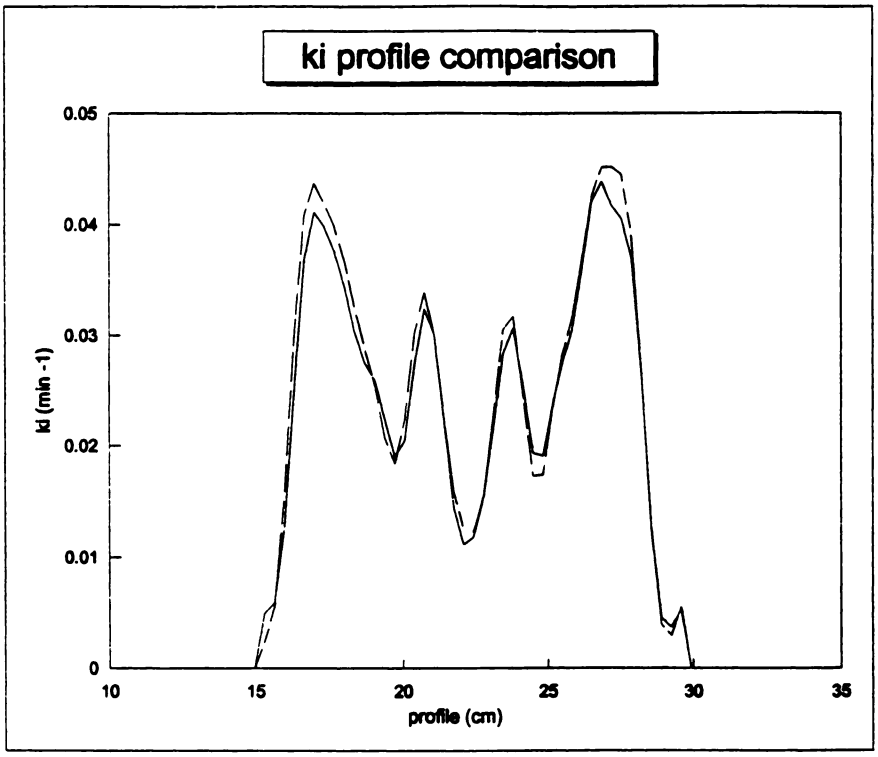

FIGURE 4. A lateral profile cut on the brain image in Figure 3 through the caudal nucleus region. Solid line = present method; dash line = graphical analysis method.

The metabolic rate $K_i(x, y)$ and total blood space image $V_d(x, y)$ are then recomputed for the entire image set using the grand estimate $\langle\langle dc_1 \rangle\rangle$:

From Equations 7 and 8,

$$K_a(x, y) = \frac{T_3(x, y)A_2 - T_2(x, y)A_3}{\langle\langle dc_1 \rangle\rangle(A_2 - A_3) + A_2 dc_2}, \quad \text{Eq. 17}$$

$$V_{da}(x, y) = \frac{\langle\langle dc_1 \rangle\rangle[T_2(x, y) - T_3(x, y)] + T_2(x, y)dc_2}{\langle\langle dc_1 \rangle\rangle(A_2 - A_3) + A_2 dc_2}. \quad \text{Eq. 18}$$

From Equations 8 and 9,

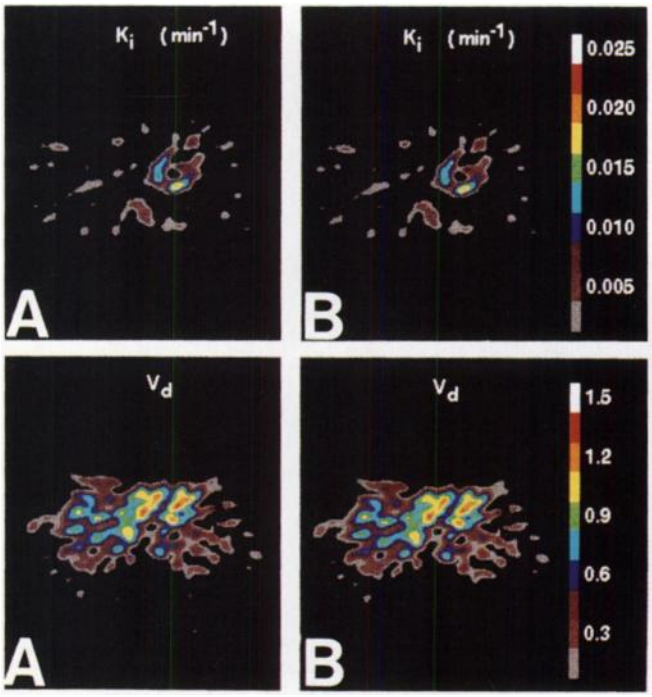

FIGURE 5. (A) K_i and V_d images derived from regular graphical analysis with continuous venous blood sampling (35 samples). (B) K_i and V_d images with this proposed method using three venous blood samples.

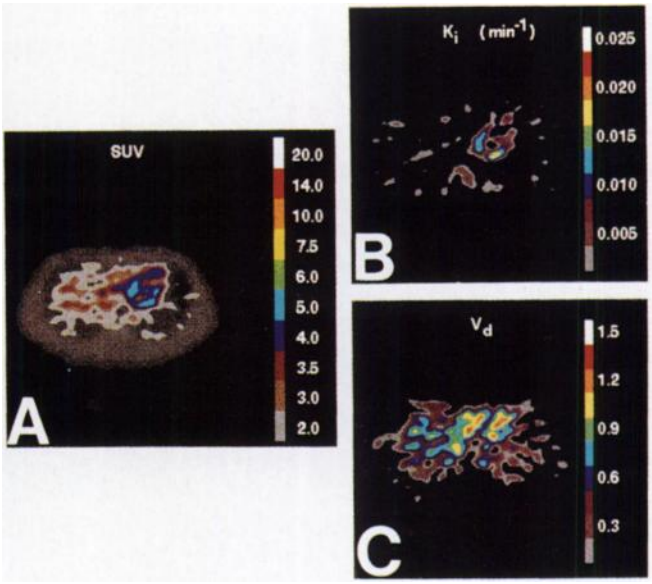

FIGURE 6. Comparison of SUV and parametric images. The K_i image shows higher contrast or dynamic range than the SUV image.

$$K_b(x, y) = \frac{[T_4(x, y)A_3 - T_3(x, y)A_4]}{\langle\langle dc_1\rangle\rangle(A_3 - A_4) + dc_2(A_3 - A_4) + A_3dc_3}, \quad \text{Eq. 19}$$

$$V_{db}(x, y) =$$

$$\frac{\langle\langle dc_1\rangle\rangle[T_3(x, y) - T_4(x, y)] + dc_2[T_3(x, y) - T_4(x, y)] + T_3(x, y)dc_3}{\langle\langle dc_1\rangle\rangle(A_3 - A_4) + dc_2(A_3 - A_4) + A_3dc_3} \quad \text{Eq. 20}$$

From Equations 7 and 9,

$$K_c(x, y) = \frac{T_4(x, y)A_2 - T_2(x, y)A_4}{\langle\langle dc_1\rangle\rangle(A_2 - A_4) + dc_2A_2 + dc_3A_2}, \quad \text{Eq. 21}$$

$$V_{dc}(x, y) =$$

$$\frac{\langle\langle dc_1\rangle\rangle[T_2(x, y) - T_4(x, y)] + dc_2T_2(x, y) + dc_3T_2(x, y)}{\langle\langle dc_1\rangle\rangle(A_2 - A_4) + dc_2A_2 + dc_3A_2}. \quad \text{Eq. 22}$$

The final parametric images of $K_i(x, y)$ and $V_d(x, y)$ are computed from the average as follows.

$$K_i(x, y) = [K_a(x, y) + K_b(x, y) + K_c(x, y)]/3, \quad \text{Eq. 23}$$

$$V_d(x, y) = [V_{da}(x, y) + V_{db}(x, y) + V_{dc}(x, y)]/3. \quad \text{Eq. 24}$$

RESULTS

This method was tested for FDG PET applications on six normal brains and two chest studies (heart, liver and tumor) with 10 mCi of FDG injected. Three serial time scans (15 min each) were acquired after a waiting period of 10 min. During the six brain studies and one chest study, continuous blood samples (once every minute for the first 7 min and then every 5 min up to the end of the study) were obtained so the present method (using three of the blood samples) could be compared with the findings from the graphical analysis method (using all blood samples). Arterialized venous blood sampling was from the hand. The

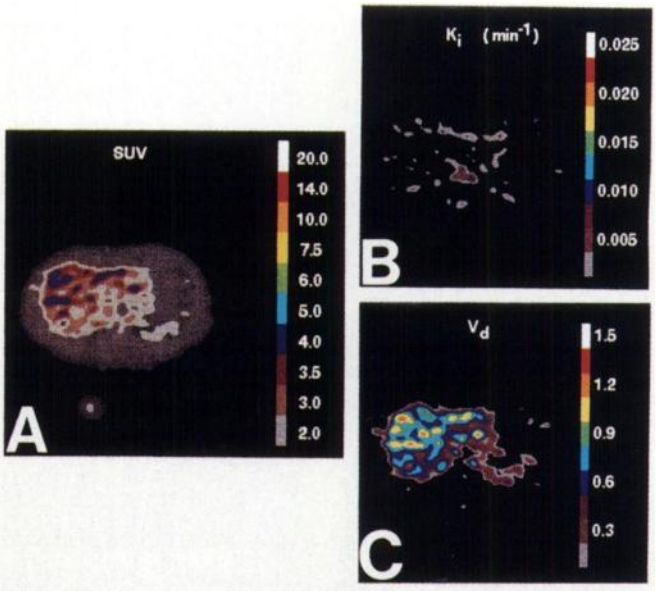

FIGURE 7. Comparison of SUV and parametric images of a liver.

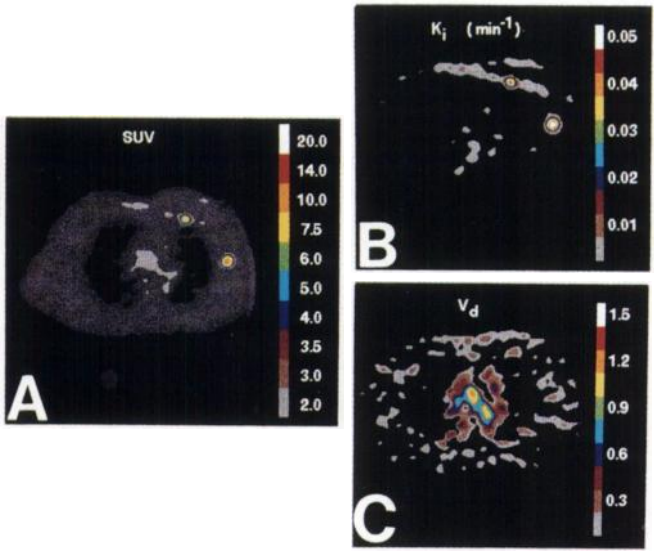

FIGURE 8. Breast cancer study.

number of pixels selected by the constraints to estimate dc_1 was large (>10,000) for 21 slices. The results of unconstrained computations were found to be unacceptable. The total computation time to generate 21-slice K_i and V_d images was about 30 sec on an IBM RS/370 Workstation with a nonoptimized computer program (Armonk, NY). These results are shown in Figs. 2 to 8.

A direct computation of dc_1 (individual pixel dc_1 without the averaging described), K_i and V_d (Equations 10–12) produced noisy parametric images (Fig. 2B) because of the large errors in the derived dc_1 (individual pixel). With the proposed method, using the fact that the initial blood integral $dc_1(x, y)$ was about the same for all pixels and thus computing the grand mean $\langle\langle dc_1\rangle\rangle$, the quality of the parametric images of K_i and V_d was considerably better (Fig. 2A). The measured K_i from the parametric images (Fig. 2A) showed that gray matter has a FDG metabolic rate in the range of 0.03 to 0.04/min and that white matter has about 0.005 to 0.01/min. These values agreed with published data (*2,3,5,7*).

Figure 3 illustrated good agreement between the regular graphical analysis and the proposed analysis for a PET-FDG brain study. A profile cutting across the brain images in Figure 3 is shown in Figure 4 to show the comparison more accurately. The average errors in K_i and V_d (present method relative to the graphic method) derived from averaging the percentage errors (absolute error) per pixel over all the pixels in the entire brain is shown in Table 1 for six brains (K_i threshold at 0.008) and a heart study (K_i threshold at 0.001). The errors in dc_1 are also included in Table 1. These comparisons showed that the proposed method agreed with the graphical method well in K_i and less well in V_d and the derived dc_1. Apparently, the derived K_i was not highly sensitive to the errors in the derived blood input dc_1; the error in V_d had the same magnitude as that of dc_1. The three cases (Brains 1, 2 and 3 in Table 1) with the smallest

TABLE 1
Average Absolute Errors per Pixel Relative to Graphical Analysis

Errors	Brain 1	Brain 2	Brain 3	Brain 4*	Brain 5*	Brain 6†	Heart‡
dc_1	4.6%	5.4%	3.2%	14.4%	20%	38%	9.7%
K_i	3.2%	3.6%	3.1%	4.3%	8.0%	7.1%	1.5%
V_d	8.5%	7.3%	11.4%	17.4%	18%	33%	15.3%

*Minor head movement was reported during scans.
†Significant head movement was reported during scans.
‡Ungated heart studies with normal heart movements.
dc_1 = blood integral variable; K_i = macrometabolic rate constant; V_d = volume of distribution.

dc_1 and V_d errors coincided with the fact that the subjects reported no movement (or sleeping) during the studies; the studies with larger dc_1 errors coincided with reported subject movements during the imaging periods (especially Brain 5 in Table 1). Hence, the average K_i error of this method relative to the graphical analysis method was found to be about 3%–4%, except in the cases of large patient movement. The average V_d error was higher at 7%–15%.

The heart study is shown in Figure 5. Again the agreement between the regular graphical method (*6,7*) and the proposed method was good. If the proposed constraint, i.e., that all pixels have the same blood integral dc_1, was not used, the computed K_i image was noisy, as in the brain study (Fig. 2B) because the individual pixel dc_1 cannot be computed reliably as a result of noise in the uptake images. This constraint of identical dc_1 over all pixels improves the K_i image considerably. This dc_1 constraint is also implicitly used by other modeling methods using continuous blood sampling. In the regular graphical analysis (Fig. 5A), the K_i image is also good quality because the blood integral dc_1 is measured directly by frequent blood sampling. The average K_i for the myocardium was 0.02/min with 16 hr of fasting.

DISCUSSION

A method was presented that is clinically practical and computationally simple for acquiring parametric images of the macrometabolic rate K_i of tracers (to bound tissue spaces) and the apparent blood space V_d. This method requires only three serial scans and three blood samples at the midpoint of each scan. For a tracer such as FDG, which has a low extraction fraction, the three blood samples can be taken from the venous side with arterialization of the venous blood. The whole procedure lasts 1 hr after the injection of FDG, which is about the same as the conventional autoradiographic method. However, the autoradiographic method requires continuous blood plasma sampling, which is tedious in a busy clinical environment. Furthermore, the autoradiographic method requires an assumed set of rate constants that should be close to those of the target tissue to minimize error. For tumor applications, such an assumption, i.e., using normal tissue rate constants for all the tissue in the image, including tumors, may induce higher errors in tumors.

Compared with a nonquantitative PET-FDG study, the only extra overhead of the proposed quantitative parametric imaging method was (1) three arterialized venous blood samples and (2) about 2–3 sec of additional computation per slice, which is acceptable for routine clinical PET examinations. Preliminary results with FDG indicate that the proposed method may be as accurate as more elaborate modeling methods, and the potential that this method can be used routinely in a clinical environment is high. However, patient movement should be minimized if more accurate blood space V_d is needed. The optimal K_i threshold for computing dc_1 may be a function of the quantity and quality of the image data, which includes organ uptake, image noise, camera quantitative accuracy and well counter calibration accuracy. Other clinical PET sites and organ sites may have a different optimal K_i threshold, which can be empirically determined locally with preliminary studies by varying the K_i threshold until the derived dc_1 agrees with the true dc_1 measured by continuous blood sampling data in these preliminary studies.

The proposed method produces images that are potentially more useful than SUV images for visual and quantitative applications (Fig. 6). In the heart study, the myocardial K_i image had higher contrast from the background than did the SUV image (Fig. 6). The lower contrast SUV myocardial image was caused by high blood-pool activity in the heart area coupled with low FDG uptake in the heart (low blood glucose level from prolonged fasting). The cardiac K_i image improves the image contrast because it filters out the nearby blood pool (V_d) component. The liver study (Fig. 7A) showed high SUV values (SUV > 4.0) for normal hepatic tissue even 50 min postinjection, which could potentially obscure tumor detection (SUV > 3) in the liver. The hepatic K_i and V_d images in Figure 7B and C indicated that all the areas of high radioactivity seen in the SUV image were from the blood pool or exchangeable space contributions and were not metabolic in nature. Hence, smaller, lower activity tumors may be visualized more easily in the K_i image of the liver. A breast cancer study, with a primary tumor and an axillary metastasis, was also performed. The results are shown in Figure 8.

As in the graphical analysis method (*6,7*), the potential

shortcoming of this method is that the tissue "trap" compartment may be leaky ($k_4 \gg 0$), which leads to an underestimation of K_i and an overestimation of V_d. In such cases, the demanding compartmental nonlinear curve-fitting method to find $k_1 - k_4$ (*2,3*) would be more accurate.

ACKNOWLEDGMENTS

The authors thank E. Edmund Kim, MD, Donald A. Podoloff, MD, and Thomas P. Haynie, MD, for providing the PET center resources and support for this project. They also thank Roy Tilbury and Wayne Tansey for the FDG preparation, Wayne Tinsey for blood counting and Bill Broussard for technical assistance. This project was supported in part by National Institutes of Health grant RO1-CA58980-01 and the University of Texas M. D. Anderson Cancer Center PRS grant 4-0020914.

REFERENCES

1. Sokoloff L, Reivich M, Kennedy C, et al. The (^{14}C)-deoxyglucose method for the measurement of local cerebral glucose utilization: theory, procedure and normal values in the conscious and anesthetized albino rat. *J Neurochem* 1977;28:897–916.
2. Phelps ME, Huang SC, Hoffman EJ, et al. Tomographic measurement of local cerebral glucose metabolic rate in human with (F-18)2-fluoro-2-deoxy-D-glucose: validation of method. *Ann Neurol* 1979;6:371–388.
3. Huang SC, Phelps ME, Hoffman EJ, et al. Noninvasive determination of local cerebral metabolic rate of glucose in man. *Am J Physiol* 1980;238:E69–E82.
4. Brooks RA. Alternative formula for glucose utilization using labelled deoxyglucose. *J Nucl Med* 1982;23:528–539.
5. Hutchins GD, Holden JE, Koeppe RA, et al. Alternative approaches to single scan estimation of cerebral glucose metabolic rate using glucose analogs, with particular application to ischemia. *J Cereb Blood Flow Metab* 1984;4:35–40.
6. Patlak CS, Blasberg RG, Fenstermacher JD. Graphical evaluation of blood-to-brain transfer constants from multiple time uptake data. *J Cereb Blood Flow Metab* 1983;3:1–7.
7. Gjedde A. Calculation of glucose phosphorylation from brain uptake of glucose analogs in vivo: a re-examination. *Brain Res Rev* 1982;4:237–274.
8. Hutchins GD, Hichwa RD, Koeppe RA. A continuous flow input function detector for $H_2{}^{15}O$ blood flow studies in positron emission tomography. *IEEE Trans Nucl Sci* 1986;NS-33:546–549.
9. Eriksson L, Holte S, Bohm C, Kesselberg M, Hovander B. Automated blood sampling systems for positron emission tomography. *IEEE Trans Nucl Sci* 1988;NS-35:703–707.